Interface Electric Field of Carbon Black Loaded Electrode and Its Significant Influence on Charge Injection into Polyethylene

Chun Xiao, Yewen Zhang, Zhenlian An, Feihu Zheng, Wenjie Wei, Huayun Xuan

Shanghai Key Laboratory of Special Artificial Microstructure Materials and Technology, Pohl Institute of Solid State Physics, Tongji University, 1239 Siping Road, Shanghai, 200092, People's Republic of China

Received 16 December 2010; accepted 24 May 2011
DOI 10.1002/app.34950
Published online 1 September 2011 in Wiley Online Library (wileyonlinelibrary.com).

ABSTRACT: Experimental results show that much more charge injection occurs from nanocarbon black loaded ethylene-vinyl acetate copolymer semiconductor electrode (semiconductor electrode for short) into polyethylene (PE) than that from metal electrodes, which cannot be well explained from the existing viewpoints. To explain it, the difference in interface electrical contact between the semiconductor electrode/PE and metal electrode/PE is emphasized. The interface electrical field of the semiconductor electrode with PE is quasi-quantitatively evaluated, based on a proposed model electrode composed of orderly arranged conductive spheres and ideal filling dielectric, whose interface electrical field was calculated by the finite element method. The calculation results show that the field strength near the top of the conductive spheres is much higher than the uniform strength between two ideal plane electrodes, depending on the filling rate and the size of the conductive spheres. A high filling rate of the conductive spheres is favorable to decrease the maximum interface field, and the strong field range can be effectively reduced by decreasing the size of the conductive spheres. The simulation results give a qualitative satisfactory explanation of the much more charge injection for the sample with the semiconductor electrode than those for the samples with metal electrodes from the point of view of the interface electric field. © 2011 Wiley Periodicals, Inc. J Appl Polym Sci 123: 3017–3022, 2012

Key words: dielectric properties; charge transport; polyethylene; numerical simulation; finite element method

INTRODUCTION

Space charge accumulation in polymeric insulation leads to the distortion of the electric field, likely the formation of the electrical trees or local degradation, and even the breakdown of the polymeric insulation.[1–3] It is considered to originate from the charge injection from electrodes and the field-assisted thermal ionization of impurities in bulk. For a pure polymeric insulation, the former is the dominant mechanism. Accordingly, in the recent two decades, the space charge injection from electrodes has been paid a close attention and widely investigated, together with its transportation and accumulation in bulk.[4–9]

The important role of the interface between electrode and polymeric insulation in cables as the headstream of space charge injection was emphasized by various authors.[4,5,7,10–13] The different combinations of electrode materials as cathode and anode were found to present the different charge injection behaviors and space charge accumulations in bulk even for the same polymeric insulation.[7] The difference in work function of electrode materials is easily considered to one of the causes, because it produces the different charge injection potential barrier between electrode and polymeric insulation and thus influences the charge injection. Some relationship can indeed exist between work function and electron injection rate, however, it does not provide an explanation for hole injection. But normally, anode material with higher work function leads more hole injection from anode. Experimental data show that less hole injected from anode with higher work function.[7] Therefore, some authors proposed that the interfacial states should probably take over the work function in controlling charge injection,[4,5] and it was also found that the charge traps in the surface layer of polyethylene (PE) are significantly lowered by the diffusion of the by-products in semiconductor electrode.[14] But, the experimental results show that there is much more charge injection from the semiconductor electrode than from metal electrodes,[7] even the physical reasons are not clear yet.

The purposes of this article are to experimentally demonstrate the different charge injection behaviors between the PE sample with semiconductor electrodes and those ones with metal electrodes, and to

Correspondence to: Y. Zhang (yewen.zhang@tongji.edu.cn).
The project is supported by NSFC (Nos. 51077101 and 50807040).

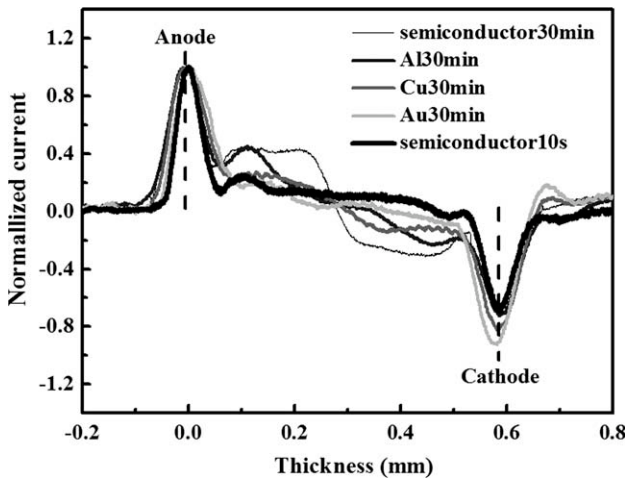

Figure 1 Space charge distributions in samples with the different electrode materials of semiconductor, Al, Cu, or Au. The width of the laser pulse is about 7 ns, and its energy is about 450 mJ.

theoretically explain the cause for the difference from the new point of view of the interface electric field on the basis of the finite element analysis.

Charge injection from different electrodes

Linear low density polyethylene (LLDPE) used in this experimental study is the granular product LL1004 from Exxon Mobile Chemical Company. LLDPE discs with a thickness of about 0.6 mm were prepared by hot-pressing at 130°C under the pressure of 15 MPa for 12 min. Electrode materials are metals of Al, Cu, and Au or the semiconductor, which were deposited for the metals or thermally bonded for the semiconductor sheet on two sides of the LLDPE discs. The space charge profiles were measured by the pressure wave propagation method. For the samples with metal electrodes, the semiconductor sheet was also used as a laser target to prevent the metal electrode from being destructed in space charge measurement, and an elastic pulse generated in the semiconductor sheet target is transmitted to the samples.

Figure 1 shows space charge profiles of the samples with the different electrodes of semiconductor, Al, Cu, or Au applied to a direct current high voltage (DCHV) of −42 kV at 40°C for 30 min, where the space charge profile of the sample with semiconductor electrode at the just beginning (t = 10 s) of the DCHV application is also given as a reference. LLDPE was used as received in this experimental study, and the charge generated from ionization of impurities in bulk can be ignored,[15] and the charge measured in the samples come from electrode injection. The space charge profiles are normalized to their anode signals, respectively, to compare their space charge injection and eliminate the influence of the elastic pulse strength in samples, which should be different between the sample with semiconductor electrode and the sample with metal electrode or the samples with different metal electrodes due to the interface reflection of elastic pulse and the coupling. It can be seen clearly that homocharge injection occurs at both electrodes for all the samples, however, the amount of the injected electron or hole for the sample with the semiconductor electrode is much larger than those for the samples with metal electrodes. In addition, either electron or hole is more easily injected into PE from Al electrode than Cu or Au electrode, and Au electrode injects very little. The similar results were also reported for semiconductor, Al and Au electrodes,[7] although there are some discrepancies in space charge distribution and its injection amount between the reported results and these results due to the differences in polymeric insulation material, thickness of samples and measurement conditions, and the possible difference in sample preparation.

Although there exists the relationship of work function order that Al (4.08 eV[16]) < Cu (4.6 eV[17]) <Au (4.8 eV[18]), it is difficult to well explain the electronic injection ranking of Al > Cu > Au as seen in Figure 1, because work function cannot provide an explanation for the hole injection that Al is also more injection for hole than Au or Cu. It is even more difficult to explain the much more electron or hole injection from the semiconductor electrode than the metal electrodes. This indicates that there is no a direct or complete relationship between work function and space charge. Although the interfacial states due to physical and chemical disorders at the contact and/or the localized states in the band gap of PE are advocated to be the possible controlling factors[4,5,19] an expectable difference in electrical contact between the semiconductor electrode/polymeric insulation and metal electrode/polymeric insulation is seldom paid attention to. The electrical contact of the former is actually formed between a lot of the conductive nano-CB particles and polymeric insulation, while that of the latter is almost the plane contact of metal electrode with polymeric insulation. This suggests that the interface electric field of the former should be quite different from that of the latter.

Model description and numerical simulation approach

The multipoint electrical contacts between PE and nano-CB loaded semiconductor electrode in a practical cable is shown in Figure 2(a), where the average diameter and volume filling rate of the CB particles are about 40 nm and 47%, respectively. The SEM picture shows that the interface between PE and

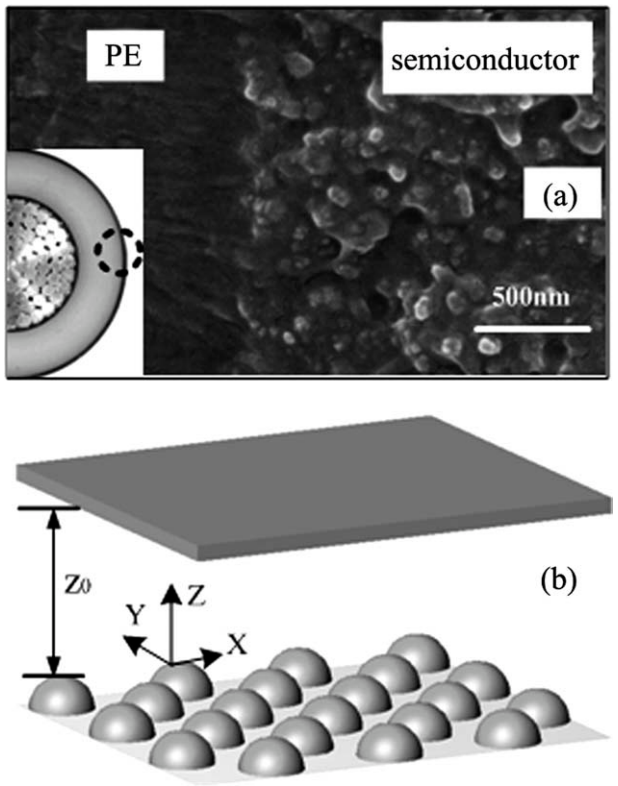

Figure 2 (a) Micrograph of the PE/semiconductor electrode interface in a practical cable and (b) model electrode surface.

semiconductor is not the smooth planar contact but composed of the many point contacts between the nano-CB particles and PE. To evaluate quasi-quantitatively, the interface electrical field, the semiconductor electrode is modeled as a network composed of the orderly arranged conductive spheres with a same size and filled with an ideal dielectric, and its surface is simplified as a layer of conductive semispheres orderly distributed on the ideal dielectric surface, as shown in Figure 2(b). In the model system, the opposite electrode to the model electrode is taken as a perfect-earthed planar electrode. A DCHV is applied between the model electrode and the planar electrode, and the charge on the model electrode can be considered to distribute only on the conductive semispheres. In addition, to simplify the numerical simulations, the medium between the two electrodes is assumed vacuum, that is, neither polarization nor space charge accumulation in dielectric is taken into account in the simulations.

COMSOL Multiphysics is a powerful tool for modeling and solving many scientific and engineering problems based on partial differential equations. It supports periodic boundary condition and can mesh the geometry automatically with high definition and calculate electrostatic field using its module of the electrostatic field. Although the numerical simulation is not restricted in principle by the number, dimension or nearest-neighbor distance of the semispheres, a large number of the semispheres can severely affect the computation time so that the simulation is actually impossible due to too heavy calculation works. According, the numerical simulations were performed for a finite element model using the finite element analysis and solver software package. Figures 3(a,b) show the finite element model and its top view in the model electrode, respectively. The radius of the spheres or semispheres and the nearest-neighbor distance of the semispheres are respectively, denoted as r and D. By adjusting the ratio value of D/r, the filling rate of the conductive spheres in the model electrode can be changed. When a DCHV (V_s) is applied between the model electrode (EFGH) and the planar electrode (ABCD), charge only distributes on the semispheres, that is, there is no charge in the ideal dielectric surface. In numerical simulations, the boundary ADEF, ABGF, BCHG, and CDEH are set to be zero charge and symmetric, and the potential of the planar electrode (ABCD) is zero. The distance between the top of semispheres and the planar electrode, Z_0, is selected to be 10 mm in numerical simulations, considering that the thickness of insulator layer in a practical cable is usually 10–20 mm. Since the program would stop simulating when $Z_0 > 1000r$ due to too heavy calculation works, in these cases the planar electrode is replaced by an imaginary planar electrode located at from the top of semispheres, which is parallel to the planar electrode and has the potential of V_e, given by eq. (1).

$$V_e = \frac{Z_0 - 1000r}{Z_0} \cdot V_s. \tag{1}$$

The use of the imaginary planar electrode is feasible because the electric field is almost uniform at the positions larger than $10r$ from the semispheres and the relative errors caused by the replacement are <1%.

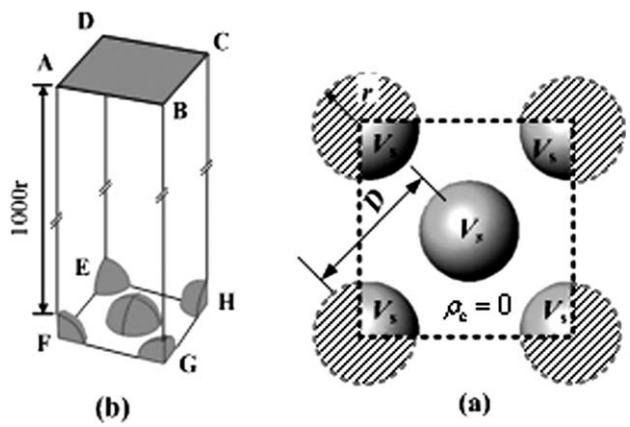

Figure 3 (a) Finite element model and (b) its top view.

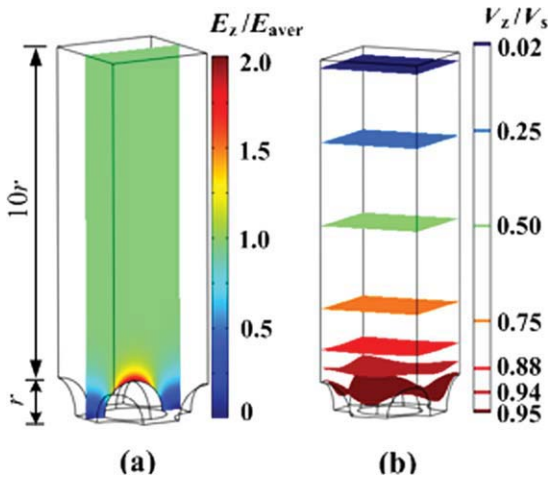

Figure 4 (a) Space electric fields and (b) potential distributions. [Color figure can be viewed in the online issue, which is available at wileyonlinelibrary.com.]

Simulation results of interface electric field

Figure 4 shows the simulation results for the case of $r = 40$ nm and $D/r = 2.28$ with a corresponding filling rate of 50% of the conductive spheres, which nearly corresponds to the case of the semiconductor electrode. In Figure 4, the space electric fields and potential distributions near the semisphere electrode are plotted with different colors, expressing the different relative values of E/E_{aver} and V/V_s ($E_{aver} = V_s/Z_0$) is the average electric field strength between the model electrode and the planar electrode, and E and V denote the space electric field and potential, respectively. As shown in Figure 4(a), the field strength close to the top of the semispheres is about 2.0 times higher than the average field, while the fields between two semispheres on the ideal dielectric surface are very low, nearly zero. The equipotential surfaces almost are planes in the positions more than $2r$ far away from the top of semispheres, as seen in Figure 4(b), where the field strength is almost the average value (E_{aver}). The results also indicate the rationality of the replacement of an imaginary planar electrode for the planar electrode when $Z_0/r > 1000$.

To have a clear view of the electric field distributions near the model electrode, the results of the simulation are also shown in Figure 5, where Z denotes the distance of a plane from the top of semispheres. It can be clearly seen from Figure 5 that the field in the plane of $Z = 0$ is extremely nonuniform. The maximum field (E_{top}) locates at the top of semispheres and the strong field regions are isolated by the low field regions. However, electric field tends to be uniform as Z, and the strong field regions almost disappear when Z increases to r. The shadow regions in the plane of $Z = -0.2r$ are the cross sections of the semispheres and thus have zero field

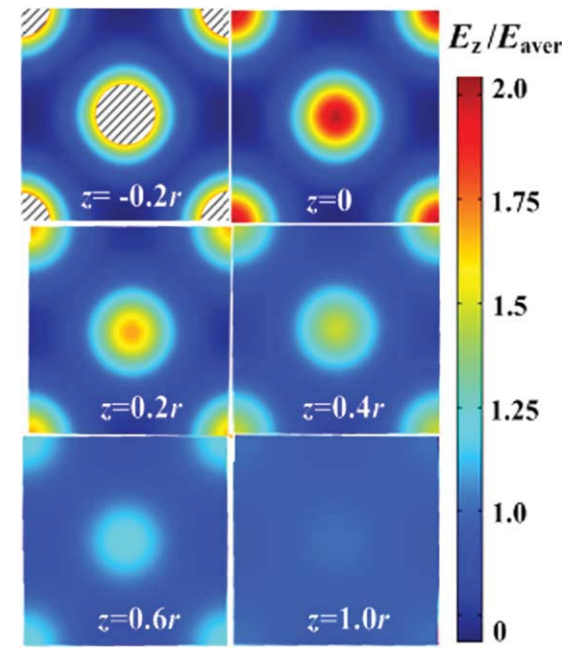

Figure 5 Electric field distributions near the model electrode. [Color figure can be viewed in the online issue, which is available at wileyonlinelibrary.com.]

strength, while the field strength close to at the edges of the cross sections is about 1.5 times higher than the average field.

Figure 6 shows the influences of the conductive sphere radius and its filling rate on the maximum field (E_{top}) at the top of the semispheres. The three filling rates of the conductive spheres were taken of 25, 50, and 74%, which correspond to the different D/r ratios of 2.87, 2.28, and 2.0, respectively. It can be seen that the maximum relative electric field strength (E_{top}/E_{aver}) presents the similar change for the three filling rates that it almost remains

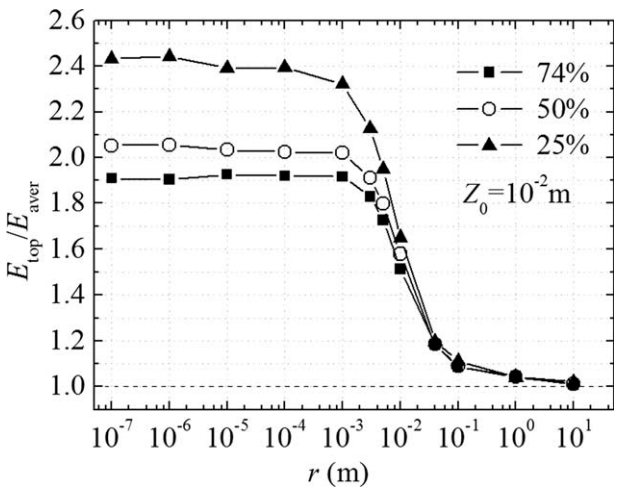

Figure 6 Dependences of the maximum relative electric field strength on conductive sphere radius and its filling rate.

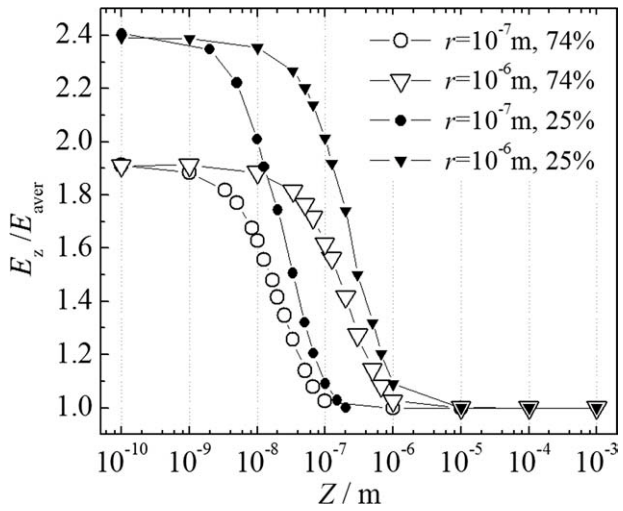

Figure 7 Electric field decays along the direction of the semisphere top.

unchanged when $r < 10^{-3}$ m and then rapidly decreases as the increase of r. And the filling rate significantly changes the maximum relative electric field. The maximum filling rate of 74%, corresponding to the case that the semispheres on the ideal dielectric surface contact with one another, leads to the minimum E_{top}/E_{aver} value of about 1.9, and the filling rate of 25% results in the E_{top}/E_{aver} value of about 2.4.

Figure 7 shows the electric field decays along the direction of the top of the semispheres for the two filling rates of 25 and 74% and the two sphere radii of 0.1 and 1 μm, respectively. The numerical simulations were carried out in a wide range of Z from very close to the top of the semispheres ($Z = 10^{-10}$ m) to far away from it ($Z = 10^{-3}$ m). It can be seen from Figure 7 that for a given filling rate, the range of enhanced field around big spheres is larger than that of small ones. Meanwhile, the local field E_z of big spheres is higher than that of small ones at the position of the same Z. As for the electrodes filled with spheres of the same size, low filling rate leads to larger the range of enhanced field, and low filling rate leads to higher local field at the position of the same Z. All above could be sum up as that higher filling rate and smaller spheres can cause lower local electric field and smaller enhanced electric field range. Besides, for all the cases, local field E_z always approaches to the average filed E_{aver} as Z gets close to r.

DISCUSSION

To check the accuracy of the simulation results or the usability of the finite element method in simulating a complicated electrostatic field, the finite element method was also used in simulating the electric field of the needle-plate electrode system shown in the inset of Figure 8, where the shape of the needle is quantified to a rotating hyperboloid expressed as eq. (2).

$$\frac{z^2}{a^2} - \frac{x^2 + y^2}{b^2} = 1. \tag{2}$$

The field strength at the needle tip can be exactly expressed by eq. (3),[20]

$$E_{tip} = \frac{2V_{tip} \cdot \sqrt{1 + r/Z_0}/r}{\ln\left[\left(\sqrt{1 + r/Z_0} + 1\right)/\left(\sqrt{1 + r/Z_0} - 1\right)\right]}, \tag{3}$$

where, V_{tip} is the electric potential of the needle, and r defined by eq. (4) and Z_0 are the radius of curvature of the needle tip and the distance between the needle tip to the plate, respectively.

$$r = b^2/a, \tag{4}$$

If $Z_0 \gg r$, the eq. (3) can be simplified as eq. (5),

$$E_{tip} = \frac{2V_{tip}}{r \cdot \mathrm{In}(1 + 4Z_0/r)} \tag{5}$$

and the field at the needle tip can be expressed by the relative field E_{tip}/E_{aver}. The average field strength E_{aver} is defined by eq. (6) as the field strength between two plate electrodes with distance of Z_0 and potential difference of V_{tip}

$$E_{aver} = \frac{V_{tip}}{Z_0}. \tag{6}$$

Figure 8 shows the theoretical relative field E_{tip}/E_{aver} and the corresponding simulation data by the

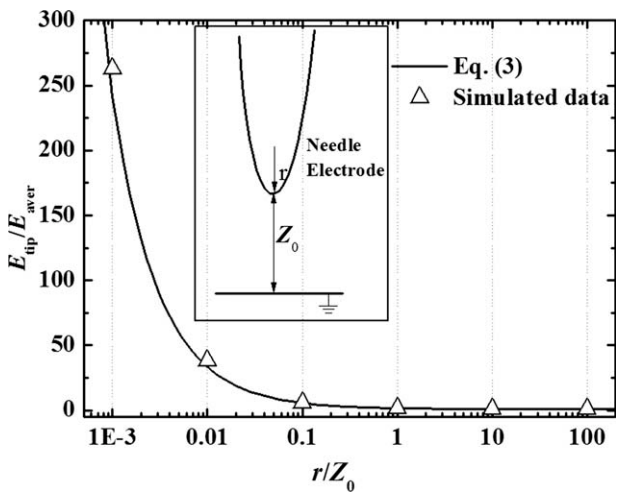

Figure 8 Comparison of theoretical curve with the simulated data for the needle-plate electrode system in the inset.

finite element method. The perfect agreement between the theoretical curve and the simulated data indicates that the finite element method is reliable to simulate a complicated electric field, like the field in this study.

Although quantitative calculation on the interface electric field of the semiconductor electrodes is impossible due to the irregular shape and distribution of the nano-CB particles, the simulation results can give at least a quasi-quantitative explanation of the much more charge injection for the sample with the semiconductor electrodes than those for the samples with metal electrodes from the point of view of the interface electric field. The interface electric fields of the semiconductor electrode nearly correspond to the simulated field shown in Figures 4 and 5, and its maximum relative electric field strength should be larger than the simulated value of about 2.0, considering that the CB particles actually are not spheres, with anomalous shapes and even tips. This means the much higher interface field for the semiconductor electrode than metal electrodes, thus rendering the more charge injection from the semiconductor electrode than from metal electrodes.

In addition, according to the simulation results shown in Figure 6, it can be concluded that such an electrode with a high filling rate and a large size of the conductive spheres is favorable to reduce the maximum interface field E_{top}. However, the significant influence of the size of the conductive spheres on the maximum interface field occurs only when $r > 10^{-3}$ m, which is much larger than the actual size of the conductive particles in semiconductor electrode in an cable system, thus the enhancement of the filling rate of the conductive spheres is a feasible and important approach to reduce the maximum interface field although it is restricted by the enwrapping capability of the polymer matrix for the conductive spheres. The evident dependence of the strong field range near the top of the semispheres on the size of the conductive spheres can be seen from Figure 7, which indicates that the strong field range can be effectively reduced by decreasing the size of the conductive spheres.

CONCLUSIONS

Experimental results demonstrate the much more charge injection for the semiconductor electrode into PE than those for the metal electrode of Al, Cu, or Au. The simulation results suggest that the interface electric field of the semiconductor electrode should be more than twice of the interface electric field of metal electrodes. Accordingly, the much more charge injection for the semiconductor electrode than metal electrodes is attributed to the much higher interface field and strong field range as well as the differences in work function of electrode materials and the possible differences in interfacial state between the semiconductor electrode/PE and the metal electrode/PE. The simulation results also indicate the dependences of the interface electric field and strong field range on the filling rate and size of conductive particles. Such an electrode with a high filling rate and a small size of conductive spheres is favorable and feasible to reduce the maximum interface field and the strong field range, thus to suppress the charge injection from electrode, which is meaningful to practical cable manufacture.

References

1. Malec, D. IEEE Trans 2007, 14, 502.
2. Dissado, L. A.; Mazzanti, G.; Montanari, G. C. IEEE Trans 1997, 4, 496.
3. Yewen, Z.; Lewiner, J.; Alquie, C.; Hampton, N. IEEE Trans 1996, 3, 778.
4. Neagu, E.; Dias, C. IEEE 2009, 25, 15.
5. Rogti, F.; Mekhaldi, A.; Laurent, C. IEEE Trans 2008, 15, 1478.
6. Montanari, G. C.; Morshuis, P. H. F. IEEE Trans 2005, 12, 754.
7. Chen, G.; Tay, T. Y. G.; Davies, A. E.; Tanaka, Y.; Takada, T. IEEE Trans 2001, 8, 867.
8. Lim, F. N.; Fleming, R. J.; Naybour, R. D. IEEE Trans 1999, 6, 273.
9. Tanaka, Y.; Li, Y.; Takada, T.; Ikeda, M. J Physics D: Applied Physics 1995, 28, 1232.
10. Chen, G.; Tanaka, Y.; Takada, T.; Zhong, L. IEEE Trans 2004, 11, 113.
11. Ho, Y. F. F.; Chen, H. G.; Davies, A. E.; Swingler, S. G.; Sutton, S. J.; Hampton, R. N. IEEE Trans 2003, 10, 393.
12. Murakami, Y.; Mitsumoto, S.; Fukuma, M.; Hozumi, N.; Nagao, M. Electr Eng Jpn 2002, 138, 19.
13. Suh, K. S.; Jin, H. N.; Ji, H. K.; Kwang, C. K.; Sang, O. H. IEEE Trans 2000, 7, 216.
14. An, Z.; Xie, C.; Jiang, Y.; Zheng, F.; Zhang, Y. J Appl Phys 2009, 106, 104112.
15. Zheng, F.; Zhang, Y.; Gong, B.; Zhu, J.; Wu, C. Sci China Ser E: Eng Mater Sci 2005, 48, 354.
16. Fukunaga, K.; Maeno, T.; Hashimoto, Y.; Suzuki, K. IEEE Trans 1998, 5, 276.
17. Kar, S. Solid State Electron 1975, 18, 169.
18. Sapoval, B.; Hermann, C. Physics of Semiconductors; Springer: New York, 1995.
19. S, L. R. E. A. J Phys D: Appl Phys 2006, 39, 1427.
20. Backhaus-Ricoult, M.; Trichet, M. Solid State Ionics 2002, 150, 143.